Size-controlled synthesis of gold nanoparticles by ultrafine bubbles and pulsed ultrasound

Keiji Yasuda[a*], Tomofumi Sato[a], Yoshiyuki Asakura[b]

[a] *Department of Chemical Systems Engineering, Graduate School of Engineering, Nagoya University, Furo-cho, Chikusa-ku, Nagoya 464-8603, Japan*

[b] *Honda Electronics Co., Ltd., 20 Oyamazuka, Oiwa-cho, Toyohashi 441-3193, Japan*

Email: yasuda.keiji@material.nagoya-u.ac.jp

Abstract

Size-controlled gold nanoparticles (AuNPs) were synthesized by ultrasonic irradiation of $HAuCl_4$ aqueous solutions with the aid of ultrafine bubbles (UFBs) in the absence of any capping and reducing agents. Upon addition of air-UFBs, the mean diameter of the spherical AuNPs decreased. This result was attributed to the sonochemical reduction of gold ions in aqueous solution being accelerated by the UFBs. Moreover, the AuNPs were stable in a solution containing UFBs because AuNPs electrostatically adsorbed onto UFBs, whose lifetime in water was very long. Compared with the mean diameter of AuNPs synthesized with argon-, nitrogen- and oxygen-UFBs, that of AuNPs synthesized with air-UFBs was smaller. Pulsed ultrasound delivered with the same time-averaged power as continuous-wave irradiation further decreased the mean diameter of the AuNPs. Size-controlled synthesis of AuNPs without the use of a capping or reducing agent was successful through optimization of the number air-UFBs and the pulsed ultrasound conditions.

Keywords

Gold nanoparticles, Ultrafine bubbles, Pulse wave, Ultrasound, Size control, Colloidal stabilization

1. Introduction

Gold nanoparticles (AuNPs) have catalytic, electronic, magnetic and optical characteristics that vary with their sizes and shapes (Daniel and Astruc, 2004). They are used in light-energy conversion devices, biosensors, electric circuits and catalysis. The catalytic activity of AuNPs increases with decreasing particle size (VanBokhoven, 2008). AuNPs are also used in low-temperature solders and fine wiring because the melting point of AuNPs drastically decreases as their diameter decreases below 5 nm (Buffat and Borel, 1976). Thus, control of the size and shape of AuNPs is important for industrial applications.

The solution-based synthesis of AuNPs generally requires a gold salt, a reducing agent and a capping agent. Capping agents, which are typically surfactants and/or polymers, control particle size and improve colloid stability. However, surfactants and polymers adsorbed onto the surface of AuNPs decrease the gold purity and degrade the performance of AuNPs. In addition, reducing agents and capping agents can generate byproducts. AuNPs synthesis methods that do not involve a surfactant, polymer, or reducing agent have economic and environmental advantages because they minimize material use and operations (e.g. washing, waste treatment and recycling).

Metal nanoparticles are synthesized by ultrasonic irradiation of an aqueous solution (Koltypin et al., 1997; Caruso et al., 2002; Okitsu et al., 2005, 2009; Park et al., 2006; Sakai et al., 2009, 2014; Saliman et al., 2016; Sari et al., 2018; Takahashi et al., 2018). This formation of metal nanoparticles is attributable to ultrasonic cavitation. Sakai et al. reported that the ultrasonic method can synthesize AuNPs from an aqueous solution of $HAuCl_4$ in the absence of reducing and capping agents (Sakai et al., 2009, 2014). Nanocomposites of AuNPs and graphene without capping agents have been used as a highly sensitive amperometric sensor for the determination of trace trivalent chromium in environmental water (Sari et al., 2018). AuNPs without capping agents have also been used in the sensitive and portable colorimetric detection of insecticides (Takahashi et al., 2018). However, controlling the size and improving the colloidal stability of AuNPs are difficult without the use of

capping agents.

Small bubbles with a diameter less than 1 μm are called ultrafine bubbles (UFBs). An alternative and equivalent term for UFBs is bulk nanobubbles (Alheshibri et al., 2016). UFBs have a very long lifetime in water, where they persist for more than two months, because their buoyancy-induced rising velocity is negligible (Ebina et al., 2013). UFBs also have an electrically charged surface (Oh and Kim, 2017) and are bioactive (Liu et al., 2016). Water containing UFBs has been used in various fields, including cleaning (Zhu et al., 2016), surface treatment (Matsuno et al., 2014), agriculture (Minamikawa et al., 2015), wastewater treatment (Temesgen et al., 2017) and dietary supplements (Safonov and Khitrin, 2013). These UFBs have no shell, and the mechanism responsible for their stability is unclear (Yasui et al., 2016).

In the present study, UFBs were used to synthesize AuNPs in the absence of reducing and capping agents. Aqueous solutions of $HAuCl_4$ in the presence of UFBs were irradiated with ultrasound, and the synthesized AuNPs were characterized by scanning electron microscopy. The effects of concentration and the gas used to generate UFBs on the particle size and colloid stability of the AuNPs were examined. Moreover, pulsed ultrasound was used to irradiate the solution and the effects of the pulse-wave conditions on the particle size were investigated.

2. Experimental methods

Samples were prepared from $HAuCl_4$ (Wako, Japan) and water containing UFBs. The initial concentration of $HAuCl_4$ was 0.1 mM. Ultrapure water was produced using systems equipped with both Elix-UV20 and Milli-Q Advantage for laboratory use (Millipore). Water containing UFBs was prepared from ultrapure water by a pressurized dissolution method (ultrafineGaLF, IDEC, Japan). Air, argon, oxygen and nitrogen were used as gases to generate UFBs. The number concentration of UFBs with diameters ranging from 30 to 1000 nm was measured using a nanoparticle tracking method (NanoSight, Malvern). In this study, the mode diameters of UFBs for all gases were approximately

120 nm. For comparison, ultrapure water without UFBs was also used to prepare AuNPs.

A schematic of the experimental apparatus is shown in Fig. 1. A sample in a glass vessel was indirectly irradiated with ultrasound. The sample volume was 50 mL. A plate-type transducer (PZT, Honda Electronics, Japan) was driven using a power amplifier (1040L, ENI, USA) and a signal generator (1943, NF, Japan) at 495 kHz. The effective electric power applied to the transducer was calculated from the transducer voltage measured with an oscilloscope (TDS3014B, Tektronix, USA) and the current measured with a current probe (TCP202, Tektronix, USA). The electrical power applied to the transducer was 50 W. The ultrasonic power measured by calorimetry was 10 W. The sample temperature was 283 K. After 10 min of ultrasonic irradiation, the synthesized AuNPs were analyzed using a UV-Vis spectrophotometer (UV-1850, Shimadzu, Japan) and a scanning electron microscope (JEOL, Japan). More than 300 particles viewed in the micrographs were counted and measured to obtain the size and shape distributions of the AuNPs.

3. Results and discussion

3.1. Effect of ultrafine bubble concentration

Before ultrasonic irradiation, samples with and without air UFBs (Air-UFBs) were pale-yellow. After 10 min of irradiation, the sample colors changed to dark-red in the case of Air-UFBs and pale-purple in the case without UFBs. These color changes are attributed to the formation of AuNPs in the solutions.

The reactions that lead to AuNPs formation by ultrasonic irradiation have been described elsewhere (Caruso et al., 2002; Okitsu et al., 2005; Sakai et al., 2009, 2014). Water is pyrolyzed by ultrasonic cavitation, accompanied by the formation of hydrogen and hydroxyl radicals. Gold(III) ions in the bulk solution are reduced by reducing species such as hydrogen radicals, and a zero-valent gold atom (Au(0)) is generated. Nuclei of AuNPs (Au_n) form from zero-valent gold atoms (i.e. the nucleation process).

$$\text{Au(III)} + \text{reducing species} \rightarrow \text{Au(0)} \quad (1)$$

$$n\ \text{Au(0)} \rightarrow \text{Au}_n \quad (2)$$

The size of the AuNPs increases with the reduction of gold(I) ions on the surface of nuclei of AuNPs (growth process) (Sakai et al., 2009):

$$(2\ \text{Au(I)}, \text{Au}_n) \rightarrow (\text{Au(II)}, \text{Au}_{n+1}) \quad (3)$$

Fig. 2 shows absorption spectra of samples with and without Air-UFBs after 10 min of irradiation. The number concentration of Air-UFBs before irradiation was 5×10^9 mL^{-1}. Because the wavelength and height of peak absorbance became constant after 8 min of irradiation, we used an ultrasonic irradiation time of 10 min in subsequent experiments. The absorption spectrum of the AuNPs prepared with Air-UFBs has a sharp peak at 530 nm. This absorbance originates from surface plasmon resonance of the AuNPs (Link and El-Sayed, 1999). The peak absorbance wavelength depends on the size and shape of the AuNPs. In the case of AuNPs prepared without UFBs, the absorbance spectrum shows a broad peak at approximately 630 nm. These results indicate that Air-UFBs affect the size and shape of the AuNPs.

Electron micrographs of AuNPs synthesized with and without Air-UFBs are shown in Fig. 3(a). In the case of AuNPs prepared with Air-UFBs, the particle shape is almost spherical. In the case of AuNPs prepared without UFBs, however, some plate-like particles are also observed. The particle sizes of the AuNPs prepared with Air-UFBs are smaller than those of the AuNPs prepared without UFBs. Fig. 3(b) shows the diameter distributions of spherical AuNPs synthesized with and without Air-UFBs. The diameters of the particles prepared with Air-UFBs are small, and their distribution is narrow. The mean diameters of the particles prepared with and without Air-UFBs are 22 nm and 119 nm, respectively; the corresponding standard deviations are 6 nm and 80 nm, respectively.

The mean diameter of the spherical AuNPs is plotted against the number concentration of Air-UFBs in Fig. 4. The mean diameter decreases with increasing number concentration of Air-UFBs. The effect of the number concentration of Air-UFBs on the proportion of particle shapes is shown in

Fig. 5. In the case of AuNPs prepared without UFBs, the proportions of spheres, plates and rods are 0.86, 0.12 and 0.02, respectively. As the number concentration of Air-UFBs increases, the proportion of spherical particles increases and that of plate-shaped particles decreases. When the number concentration of Air-UFBs is 5×10^9 mL^{-1}, the proportions of spheres, plates and rods are 0.96, 0.01 and 0.03, respectively.

The size and shape of AuNPs are typically determined by competition between nucleation and growth processes. Nucleation is attributed to gold-ion reduction in bulk solution by reducing species. Growth is ascribed to gold-ion reduction on the surface of nuclei of AuNPs via a reaction between ions and nuclei. Therefore, when nucleation is dominant, new particle formation is substantial and the number of small particles increases. By contrast, when growth is dominant, particles increase in size. When gold-ion reduction occurs on a certain crystal face, plate-like particles are formed (Sakai et al., 2009). Because the particle size and the proportion of plate-like particles decrease with increasing UFB concentration, UFBs accelerate gold-ion reduction in bulk solution and the nucleation of AuNPs is enhanced. The effect of UFBs is explained as follows. When UFBs are irradiated by ultrasound, they increase in size through rectified diffusion (Louisnard and Gomez, 2003) with expansion and compression until the UFBs induce cavitation (Yasuda et al., 2019). Therefore, UFBs enhance cavitation. The concentration of reducing species increases because of this increase in cavitation. Moreover, negatively charged gold ions such as $[Au(III)Cl_4]^-$ electrostatically adsorb onto UFBs because the surface charge of UFBs is positive when the pH of the sample is 3.5 (Takahashi, 2005). Gold ions on the UFB surface are susceptible to chemical reduction because UFBs grow to form cavitation bubbles.

Fig. 6(a) shows photographs of AuNP colloids prepared with and without Air-UFBs. The number concentration of Air-UFBs before synthesis was 5×10^9 mL^{-1}. Although AuNPs freshly synthesized both with and without Air-UFBs were dispersed in the solution, the AuNPs prepared without UFBs almost completely precipitated after two days. By contrast, the AuNPs prepared with Air-UFBs were stably dispersed in solution after two days and remained stable for more than 2 months.

These results indicate that UFBs are also effective for dispersion stabilization of AuNPs in solution. The stabilization mechanism is illustrated in Fig. 6(b). The surface charge of AuNPs is negative because $[Au(I)Cl_2]^-$ ions adsorb onto the surface of the AuNPs as a consequence of the diffuse electric double layer (Weiser, 1933). Because the UFBs in this solution are positively charged, AuNPs electrostatically adsorb onto the UFB surface and become stable in solution. UFBs have a very long lifetime in water because their rising velocity is lower than velocity of Brownian motion. Electrostatic repulsion between UFBs prevents aggregation and coalescence of AuNPs. As a consequence of these mechanisms, AuNPs prepared with Air-UFBs are stable in solution. When we changed the solution pH to 4.5, which is the isoelectric point of the UFBs (Takahashi, 2005), the colloid became unstable and the AuNPs precipitated. Thus, the electrostatic repulsion force among UFBs plays an important role in stabilizing of AuNPs in solution.

3.2. Effects of different gases inside ultrafine bubbles

Argon (Ar), nitrogen (N_2) and oxygen (O_2) gases were also used as the gas inside UFBs and as the gas phase in the reaction vessel. The gas dissolved in the sample was replaced by each gas. The initial number concentration of each UFB was approximately 5×10^9 mL^{-1}. After ultrasonic irradiation, the colors of the AuNP colloid samples changed to red with Ar-UFBs, red with O_2-UFBs and purple with N_2-UFBs. The proportions of spherical AuNPs, as determined from electron micrographs, were 0.92 with Ar-UFBs, 0.93 with O_2-UFBs and 0.95 with N_2-UFBs. These values are slightly lower than that with Air-UFBs (0.96).

Fig. 7 shows the diameter distributions of spherical AuNPs synthesized with Ar-, O_2-, N_2- and Air-UFBs. The mean diameters are 49 nm with Ar-UFBs, 43 nm with O_2-UFBs, 73 nm with N_2-UFBs and 22 nm with Air-UFBs. The standard deviations of the diameters are 14 nm with Ar-UFBs, 8 nm with O_2-UFBs, 21 nm with N_2-UFBs and 6 nm with Air-UFBs. Thus, the AuNPs synthesized with Air-UFBs exhibit the smallest particle size and the narrowest size distribution. By contrast, the

AuNPs synthesized with N_2-UFBs are large particles with a broad size distribution.

When air-dissolved water is irradiated with ultrasound, nitrogen, oxygen and hydroxyl radicals are generated by pyrolysis of N_2, O_2 and water, respectively. Nitrous acid (HNO_2) is formed by the reaction of nitrogen, oxygen and hydroxyl radicals. Hydrogen peroxide (H_2O_2) is also formed by mutual reaction of hydroxyl radicals. Because nitrous acid and hydrogen peroxide are reducing species, they can reduce gold ions and generate AuNP nuclei, as shown in reactions (1) and (2). In addition to hydrogen radicals, reducing species such as hydrogen peroxide and nitrous acid, which are formed by ultrasonic cavitation in air-dissolved water, enhance the formation of fine and uniform AuNPs. Compared with the maximum pyrolysis temperature induced by ultrasonic cavitation of N_2 and O_2, that induced by ultrasonic cavitation of Ar is higher because a monoatomic molecule has a high ratio of specific heat (Neppiras, 1980). Because air contains N_2, O_2 and Ar, ultrasonication in water with Air-UFBs generates various reducing species. However, in the case of ultrasonication of N_2, the concentrations of formed reducing species are low and particle growth is enhanced because the solubility of N_2 in water is lower than that of O_2 and the maximum temperature inside collapsing cavitation bubbles is lower than that in the case of Ar.

3.3. Effect of pulsed ultrasound

To further decrease in the size of AuNPs, we used pulsed ultrasound (Casadonte et al., 2005, Zheng and Yasuda, 2011). The pulse duty factor was set to be 50%, and the electrical power applied to the transducer during pulse duration (pulse-on time) was 100 W, matching time-averaged power (50 W) of a continuous wave. The total time of ultrasonication of pulsed waves was equal to that of a continuous wave. Fig. 8 (a) shows electron micrographs of AuNPs synthesized with and without Air-UFBs by pulsed ultrasound. The pulse-on time was 2 ms. Almost all of the AuNPs are spherical. The particles generated with Air-UFBs are smaller than those generated without UFBs. The diameter distributions of spherical AuNPs are shown in Fig. 8 (b). The mean diameters are 13 nm for the

AuNPs prepared with Air-UFBs and 55 nm for those prepared without UFBs, and the corresponding standard deviations are 6 nm and 9 nm, respectively. As the mean diameter of AuNPs prepared with continuous-wave in the presence of Air-UFBs was 22 nm, as shown in Fig. 3, the use of a pulsed ultrasonication can further decrease in the size of the AuNPs.

Fig. 9 shows the effect of pulse-on time on the mean diameter of spherical AuNPs synthesized with Air-UFBs by pulsed ultrasound. The pulse duty factor was 50%. The dotted line indicates the mean diameter of AuNPs prepared with Air-UFBs by continuous-wave irradiation. When the pulse-on time was 0.2 ms, few AuNPs were observed. The mean diameter of AuNPs decreased as the pulse-on time was increased from 0.5 to 2 ms. To further examine this effect, we irradiated a potassium iodide (KI) aqueous solution containing Air-UFBs using pulsed ultrasound. The potassium iodide aqueous solution was used to evaluate the sonochemical reaction on the basis of triiodide (I_3^-) ions generated by ultrasonic cavitation (Koda et al., 2003). After ultrasonic irradiation, triiodide ions were detected on the basis of the absorbance at 355 nm measured using a UV−Vis spectrophotometer. When the pulse-on time was 0.2 ms, few triiodide ions were detected. As the pulse-on time was lengthened, the concentration of triiodide ions increased and became almost constant when the pulse-on time exceeded 2 ms. These results indicate that the minimum time required to induce ultrasonic cavitation was 2 ms. When the pulse-on time was shorter than 2 ms, the mean diameter of the AuNPs increased because reducing species were not fully generated and particle growth was enhanced.

However, as shown in Fig. 9, the mean diameter of AuNPs increased with increasing pulse-on time longer than 2 ms and became almost constant at pulse-on times longer than 400 ms. In particular, when the pulse-on time was greater than 20 ms, the mean diameter exceeded that of the AuNPs prepared under continuous-wave irradiation. In this experiment, the length of the pulse-on time was the same as that of the pulse-off time. Because the concentration of triiodide ions generated by ultrasonic cavitation became almost constant at pulse-on times longer than 2 ms, we investigated the influence of the pulse-off time on the mean diameter of AuNPs. The pulse-on time was fixed at 2 ms, and the pulse-off time was varied from 2 ms to 8 ms. A $HAuCl_4$ aqueous solution with Air-UFBs was

irradiated with pulsed ultrasound, and AuNPs were synthesized. The mean diameters of the AuNPs were 13 nm at 2 ms, 27 nm at 4 ms and 38 nm at 8 ms. These results indicate that the mean diameter increased with increasing pulse-off time. We found that particle growth occurred immediately after ultrasonication was stopped. We attribute the particle growth during the pulse-off time to nitrous acid and hydrogen peroxide generated during the pulse-on time. From these results, because ultrasonic power during the pulse-on time is higher than that during continuous-wave irradiation, we speculate that pulsed ultrasound generates numerous reducing species and that the generated AuNPs are small because of enhanced particle nucleation. When the pulse-off time is 2 ms, the influence of particle growth is minimized. Thus, to control the size of AuNPs, proper adjustment of the pulse-off time is important.

4. Conclusions

AuNPs were synthesized from $HAuCl_4$ aqueous solution by ultrasonic irradiation at 495 kHz, without a surfactant or reducing agent. Upon addition of Air-UFBs, the proportion of spherical AuNPs increased and the mean diameter of spherical AuNPs decreased by a factor of five (from 119 nm to 22 nm). The gold-ion reduction was speculated to be accelerated by UFBs because UFBs became nuclei of ultrasonic cavitation, enhancing cavitation generation. Moreover, AuNPs synthesized with UFBs were stable in the solution because the AuNPs electrostatically adsorbed onto UFBs and the lifetime of UFBs in water was very long. Compared with the mean diameter of AuNPs synthesized with Ar-, N_2- and O_2-UFBs, that of AuNPs synthesized with Air-UFBs was smaller because ultrasonication in water with Air-UFBs generated numerous reducing species such as hydrogen radicals, hydrogen peroxide and nitrous acid.

Pulsed ultrasound delivered with the same time-averaged power as continuous-wave ultrasound further decreased the mean diameter of the AuNPs to 13 nm when the pulse-on time was 2 ms and the duty factor was 50%. The mean diameter increased with increasing pulse-off time. We found that

cavitation and AuNP nucleation were enhanced during the pulse-on time. During the pulse-off time, the AuNPs grew. Size control of AuNPs in the absence of surfactants and reducing agents was successful through optimization of the number of UFBs and the pulsed ultrasound conditions.

Declaration of Competing Interest

The authors declare that they have no known competing financial interests or personal relationships that could have appeared to influence the work reported in this paper.

Acknowledgements

This work was supported by JSPS KAKENHI Grant Number JP19H02505.

Reference

Alheshibri, M., Qian, J., Jehannin, M., Craig, V.S.J., 2016. A history of nanobubbles, Langmuir 32(43), 11086-11100. https://doi.org/10.1021/acs.langmuir.6b02489.

Buffat, P., Borel, J-P., 1976. Size effect on the melting temperature of gold particles, Phys. Rev. A 13(6), 2287-2298. https://doi.org/10.1103/PhysRevA.13.2287.

Caruso, R. A., Ashokkumar, M., Grieser, F., 2002. Sonochemical formation of gold sols, Langumuir 18(21), 7831-7836. https://doi.org/10.1021/la020276f.

Casadonte Jr., D. J., Flores, M., Petrier, C, 2005. Enhancing sonochemical activity in aqueous media using power-modulated pulsed ultrasound: an initial study, Ultrason. Sonochem. 12(3), 147-152, doi:10.1016/j.ultsonch.2003.12.004.

Daniel, M.-C., Astruc, D., 2004. Gold nanoparticles: assembly, supramolecular chemistry, quantum-size-related properties, and applications toward biology, catalysis, and nanotechnology, Chem. Rev. 104(1), 293-346. https://doi.org/10.1021/cr030698+.

Ebina, K., Shi, K., Hirao, M., Hashimoto, J., Kawato, Y., Kaneshiro, S., Morimoto, T., Koizumi, K., Yoshikawa, H., 2013. Oxygen and air nanobubble water solution promote the growth of plants, fishes, and mice, Plos One 8(6), e65339. https://doi.org/10.1371/journal.pone.0065339.

Koda, S., Kimura, T., Kondo, T., Mitome, A., 2003, Standard method to calibrate sonochemical efficiency, Ultrason. Sonochem. 10(3), 149-156. https://doi.org/10.1016/S1350-4177(03)00084-1.

Koltypin, Y., Cao, X., Prozorov, R., Balogh, J., Kaptasc, D., Gedanken, A., 1997, Sonochemical synthesis of iron nitride nanoparticles, J. Mater. Chem. 7(12), 2453-2456. https://doi.org/:10.1039/A704008C.

Link, S., El-Sayed, M.A., 1999, Spectral properties and relaxation dynamics of surface plasmon electronic oscillations in gold and silver nanodots and nanorods, J. Phys. Chem. B 103(40), 8410-8426. https://doi.org/10.1021/jp9917648.

Liu, S., Oshita, S., Kawabata, S., Makino, Y., Yoshimoto, T., 2016. Identification of ROS produced

by nanobubbles and their positive and negative effects on vegetable seed germination, Langumir 32(43), 11295-11302. https://doi.org/10.1021/acs.langmuir.6b01621.

Matsuno, H., Ohta, T., Shundo, A., Fukunaga, Y., Tanaka, K., 2014. Simple surface treatment of cell-culture scaffolds with ultrafine bubble water, Langumir 30(50), 15238-15243. https://doi.org/10.1021/la5035883.

Minamikawa, K., Takahashi, M., Makino, T., Tago, K., Hayatsu, M., 2015. Irrigation with oxygen-nanobubble water can reduce methane emission and arsenic dissolution in a flooded rice paddy, Environ. Res. Lett. 10(8), 084012. https://doi.org/10.1088/1748-9326/10/8/084012.

Neppiras, E.A., 1980. Acoustic cavitation, Phys. Rep. 61(3), 159-251. https://doi.org/10.1016/0370-1573(80)90115-5.

Oh, S.H., Kim, J.-M., 2017, Generation and stability of bulk nanobubbles, Langumir 33(15), 3818-3823. https://doi.org/10.1021/acs.langmuir.7b00510.

Okitsu, K., Ashokkumar, M., Grieser, F., 2005, Sonochemical synthesis of gold nanoparticles: effects of ultrasound frequency, J. Phys. Chem. B 109(44), 20673-20675. https://doi.org/10.1021/jp0549374.

Okitsu, K., Sharyo, K., Nishimura, R., 2009, One-pot synthesis of gold nanorods by ultrasonic irradiation: the effect of pH on the shape of the gold nanorods and nanoparticles, Langmuir 25(14), 7786-7790. https://doi.org/10.1021/la9017739.

Louisnard, O., Gomez, F., 2003, Growth by rectified diffusion of strongly acoustically forced gas bubble in nearly saturated liquids, Phys. Rev. 67, 036610. https://doi.org/ 10.1103/PhysRevE.67.036610.

Park, J-E., Atobe, M., Fuchigami, T., 2006, Synthesis of multiple shapes of gold nanoparticles with controlled sizes in aqueous solution using ultrasound, Ultrason. Sonochem. 13(3), 237-241. https://doi.org/10.1016/j.ultsonch.2005.04.003.

Safonov, V.L., Khitrin, A.K., 2013. Hydrogen nanobubbles in a water solution of dietary supplement, Colloids Surfaces A 436, 333-336. https://doi.org/10.1016/j.colsurfa.2013.06.043.

Sakai, T., Enomoto, H., Torigoe, K., Sakai, H., Abe, M., 2009. Surfactant- and reducer-free synthesis of gold nanoparticles in aqueous solutions, Colloids Surf. A 347(1-3), 18-26. https://doi.org/10.1016/j.colsurfa.2008.10.037.

Sakai, T., Enomoto, H., Sakai, H., Abe, M., 2014. Hydrogen-assisted fabrication of spherical gold nanoparticles through sonochemical reduction of tetrachloride gold(III) ions in water, Ultrason. Sonochem. 21(3), 946-950. https://doi.org/10.1016/j.ultsonch.2013.12.010.

Saliman, M. A., Okawa, H., Takai, M., Ono, Y., Kato, T., Sugawara, K., Sato, M., 2016. Improved battery performance using Pd nanoparticles synthesized on the surface of LiFePO4/C by ultrasound irradiation, Jpn. J. J. Appl. Phys. 55(7S1), 07KE05. http://doi.org/10.7567/JJAP.55.07KE05.

Sari, T.K., Takahashi, F., Jin, J., Zein, R., Munaf, E., 2018. Electrochemical determination of chromium(VI) in river water with gold nanoparticles-graphene nanocomposities modified electrodes, E. Analy. Sci. 34(2), 155-160. https://doi.org/10.2116/analsci.34.155.

Takahashi, M., 2005. ζ Potential of Microbubbles in Aqueous Solutions: Electrical Properties of the Gas-Water. J. Phys. Chem. B 109(46), 21858-21864. https://doi.org/10.1021/jp0445270.

Takahashi, F., Yamamoto, N., Todoriki, M., Jin, J., 2018. Sonochemical preparation of gold nanoparticles for sensitive colorimetric determination of nereistoxin insecticides in environmental samples, Talanta 188, 651-657. https://doi.org/10.1016/j.talanta.2018.06.042.

Temesgen, T., Bui, T.T., Han, M., Kim, T., Park, H., 2017. Micro and nanobubble technologies as a new horizon for water-treatment techniques: a review, Adv. Colloid Interf. Sci. 246, 40-51. https://doi.org/10.1016/j.cis.2017.06.011.

VanBokhoven, J. A., 2008. Catalysis by gold: why size matters. Chimia 63(5), 257-260. https://doi.org/10.2533/chimia.2009.257.

Weiser, H.B., 1933. Inorganic Colloid Chemistry, Wiley, New York.

Yasuda, K., Matsushima, H., Asakura, Y., 2019, Generation and reduction of bulk nanobubbles by ultrasonic irradiation, Chem. Eng. Sci. 195, 455-461. https://doi.org/10.1016/j.ces.2018.09.044.

Yasui, K., Tuziuti, T., Kanematsu, W., Kato, K., 2016. Dynamic equilibrium model for a bulk nanobubble and a microbubble partly covered with hydrophobic material, Langmuir 32(43), 11101-1110. https://doi.org/10.1021/acs.langmuir.5b04703.

Zheng, X., Yasuda, K., 2011. Enhancement of sonochemical reaction by dual-pulse ultrasound, Jpn. J. Appl. Phys. 50(7S), 07HE07. DOI: 10.1143/JJAP.50.07HE07.

Zhu, J., An, H., Alheshibri, M., Liu, L., Terpstra, P.M.J., Liu, G., Craig, V.S.J., 2016. Cleaning with bulk nanobubbles, Langumir 32(43), 11203-11211. https://doi.org/10.1021/acs.langmuir.6b01004.

Figure captions

Fig. 1. Outline of experimental apparatus.

Fig. 2. Absorption spectra of samples after 10 min of ultrasonic irradiation with and without Air-UFBs.

Fig. 3. (a) Electron micrographs of AuNPs and (b) the diameter distribution of spherical AuNPs synthesized with and without Air-UFBs.

Fig. 4. Plot of the mean diameter of spherical AuNPs against the number concentration of Air-UFBs.

Fig. 5. Effect of the number concentration of Air-UFBs on the proportion of AuNPs shapes.

Fig. 6. (a) Photographs of AuNPs colloids prepared with and without Air-UFBs immediately and 2 days after synthesis. (b) Stabilization mechanism of AuNPs colloids containing UFBs.

Fig. 7. Diameter distributions of spherical AuNPs synthesized with (a) Ar-UFBs, (b) O_2-UFBs, (c) N_2-UFBs and (d) Air-UFBs.

Fig. 8. (a) Electron micrographs of AuNPs and (b) diameter distribution of spherical AuNPs synthesized by pulsed ultrasound in the presence and absence of Air-UFBs.

Fig. 9. Effect of pulse-on time on the mean diameter of spherical AuNPs synthesized with Air-UFBs by pulsed ultrasound. (dotted line: diameter of particles prepared under continuous-wave ultrasonication in the presence with Air-UFBs)

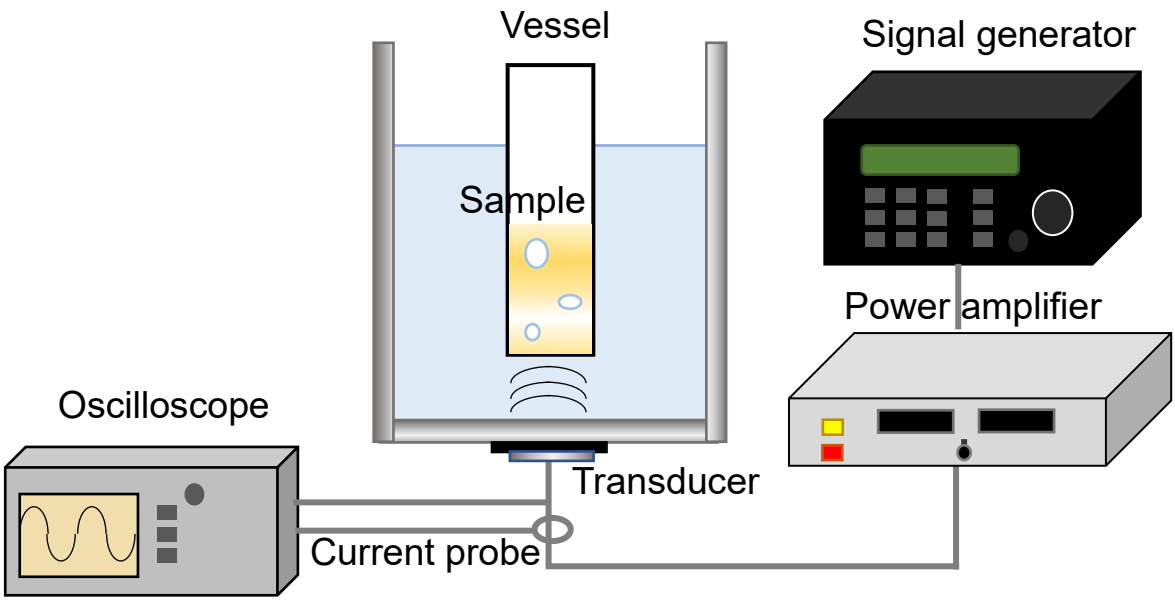

Fig. 1. Outline of experimental apparatus.

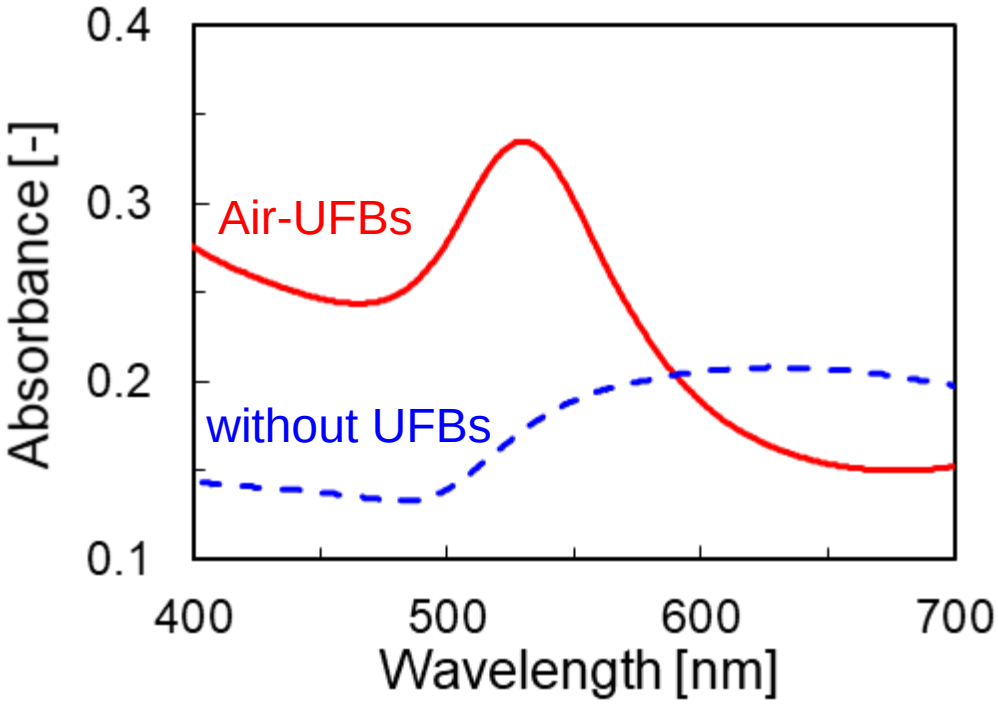

Fig. 2. Absorption spectra of samples after 10 min of ultrasonic irradiation with and without Air-UFBs.

(a)

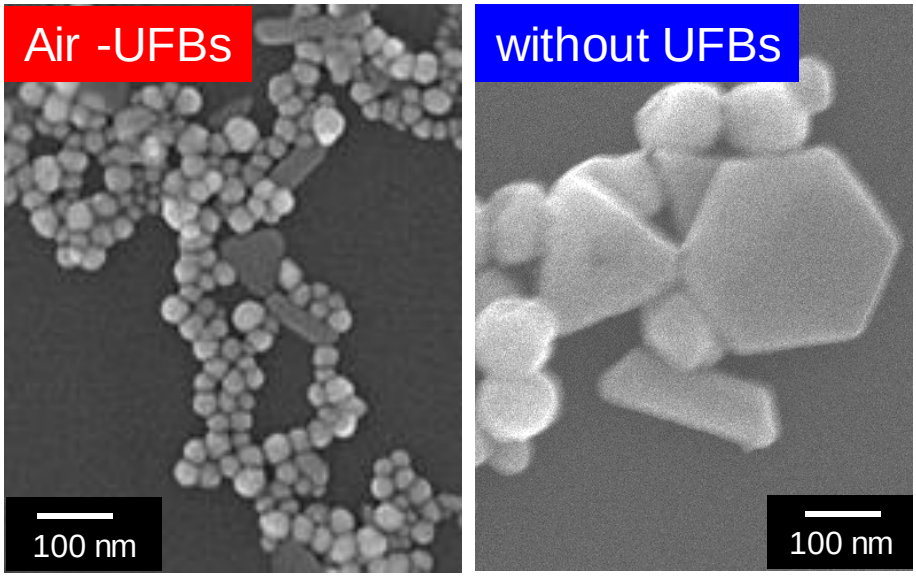

(b)

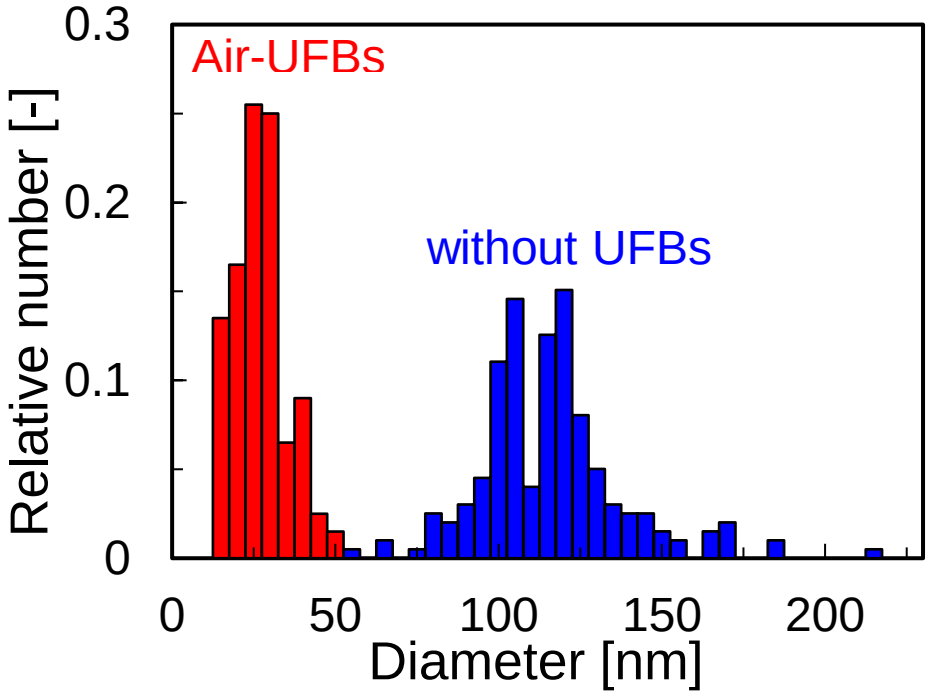

Fig. 3. (a) Electron micrographs of AuNPs and (b) the diameter distribution of spherical AuNPs synthesized with and without Air-UFBs.

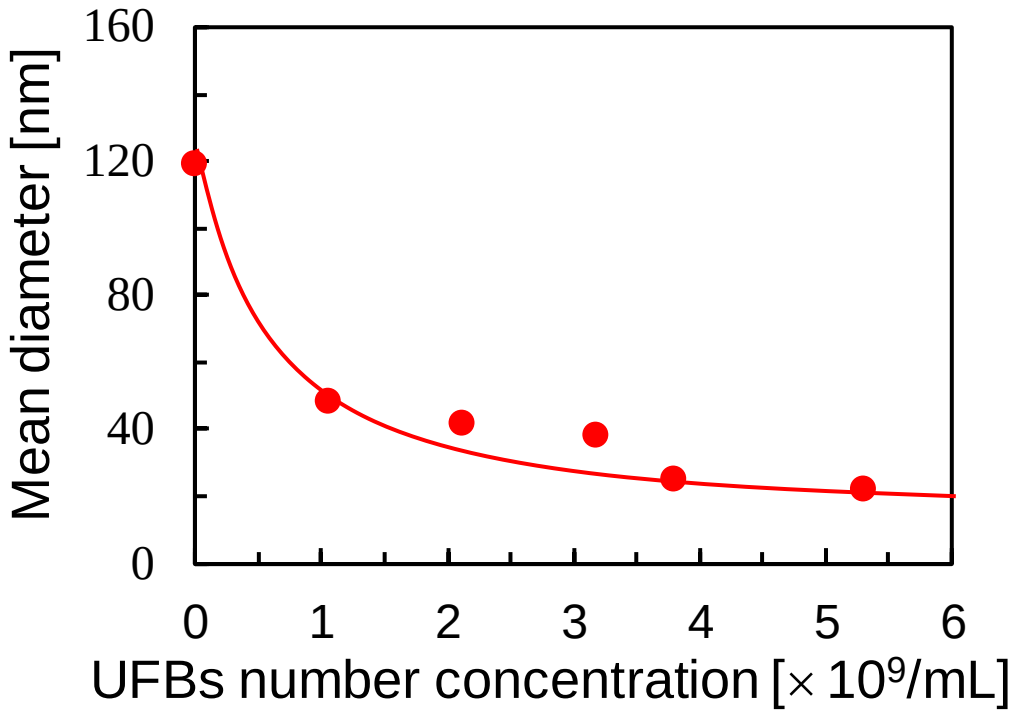

Fig. 4. Plot of the mean diameter of spherical AuNPs against the number concentration of Air-UFBs.

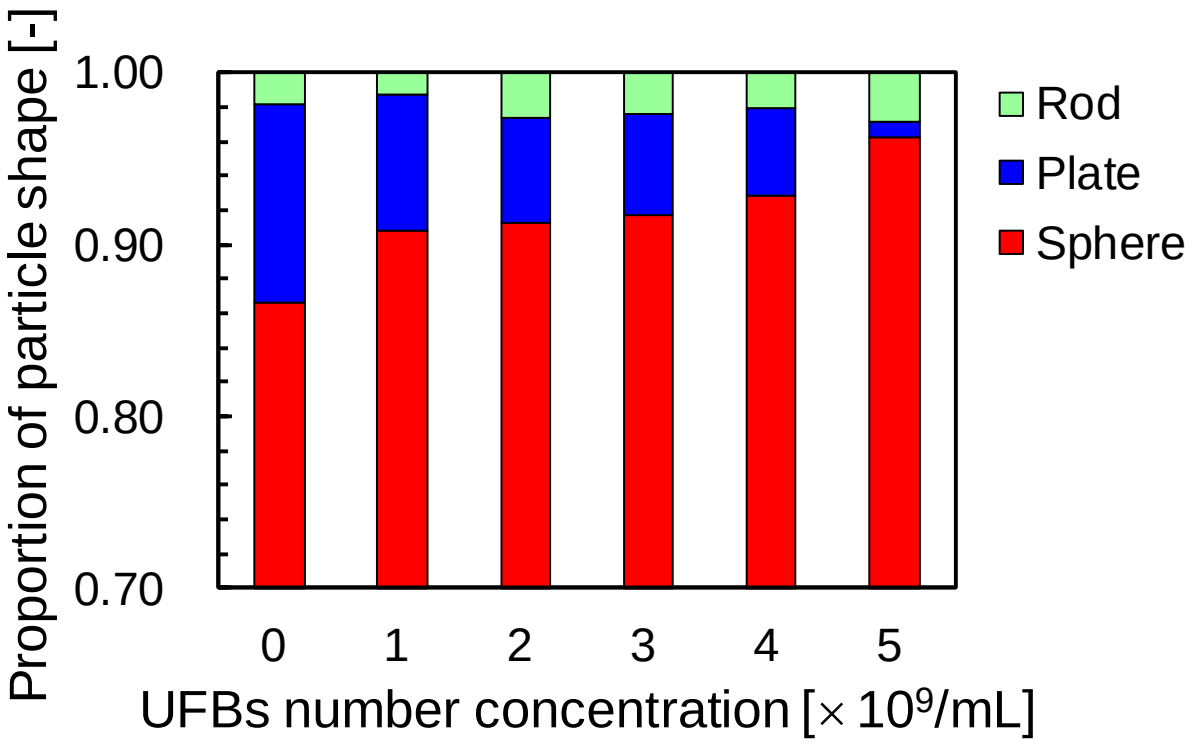

Fig. 5. Effect of the number concentration of Air-UFBs on the proportion of AuNPs shapes.

(a)

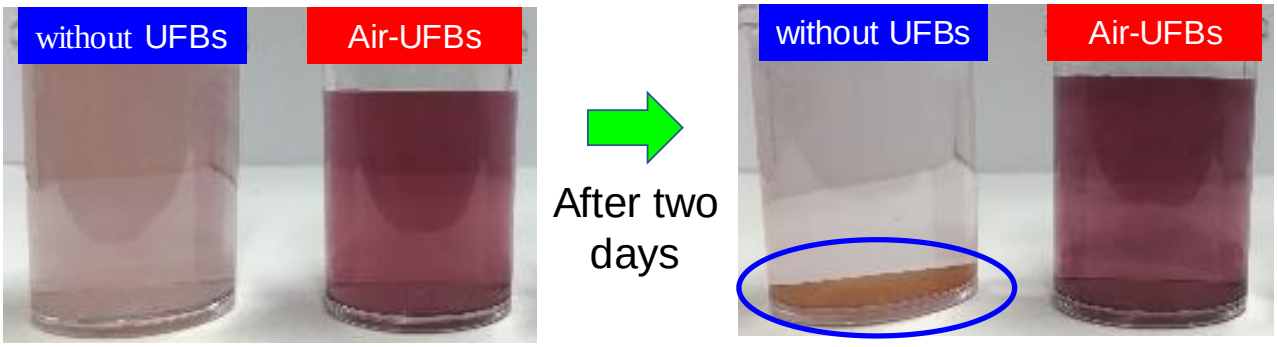

(b)

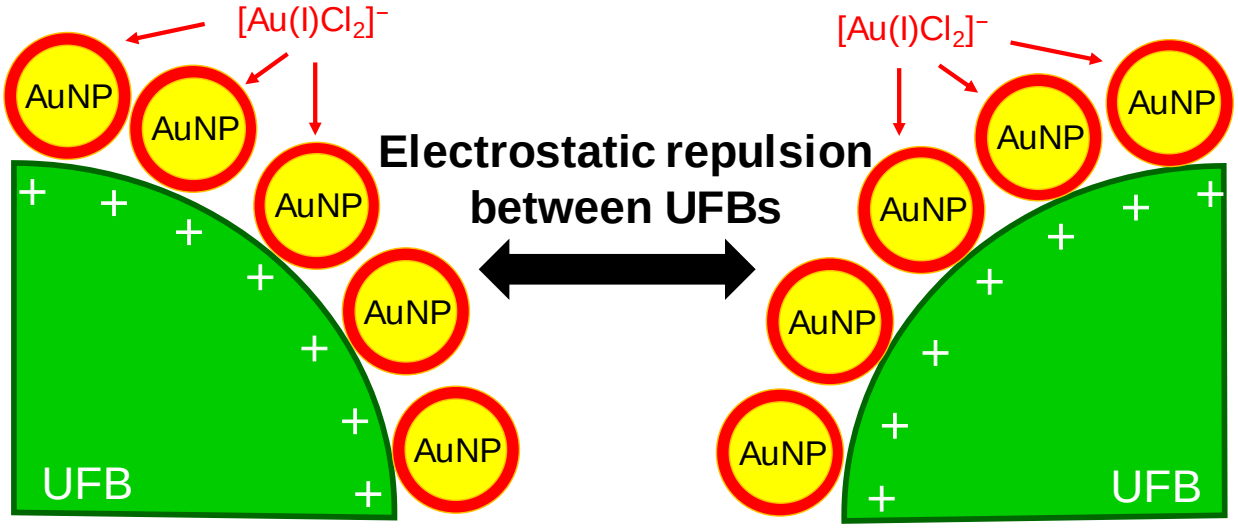

Fig. 6. (a) Photographs of AuNPs colloids prepared with and without Air-UFBs immediately and 2 days after synthesis. (b) Stabilization mechanism of AuNPs colloids containing UFBs.

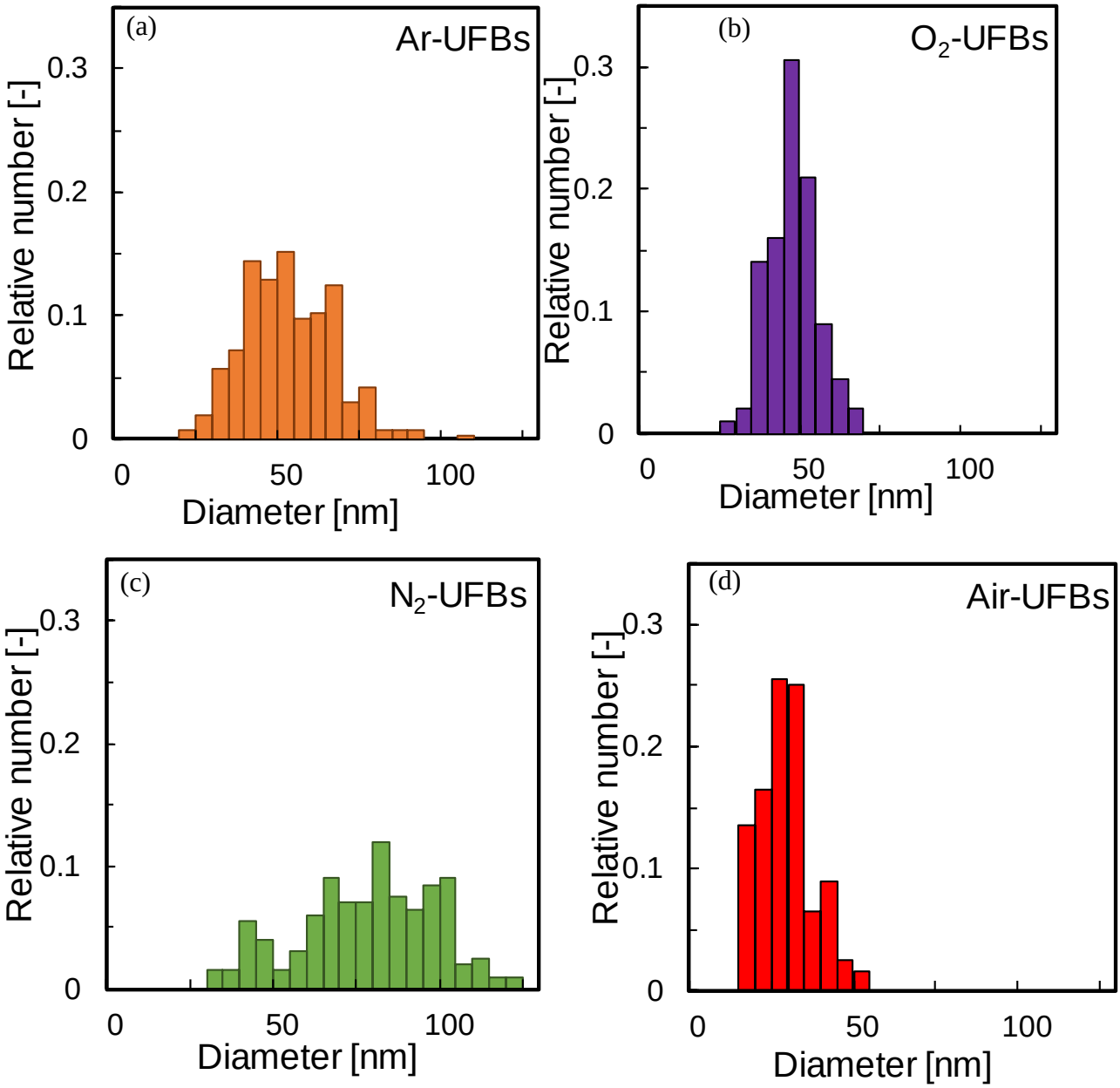

Fig. 7. Diameter distributions of spherical AuNPs synthesized with (a) Ar-UFBs, (b) O_2-UFBs, (c) N_2-UFBs and (d) Air-UFBs.

(a)

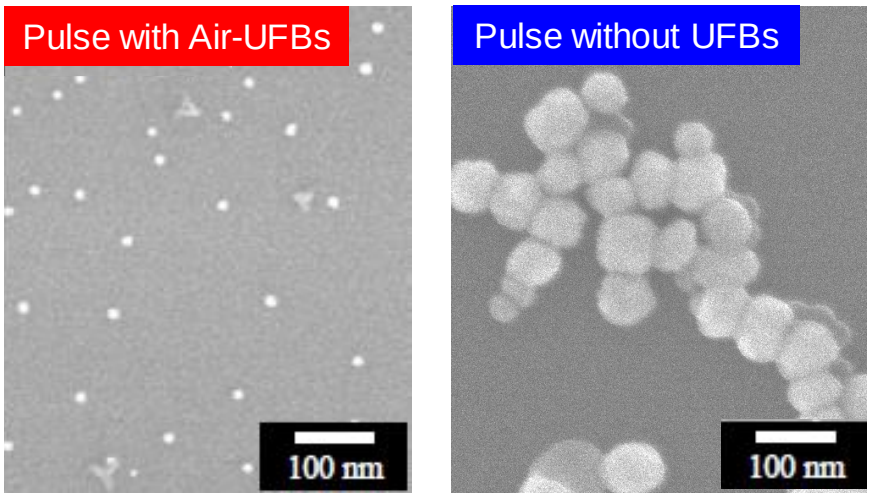

(b)

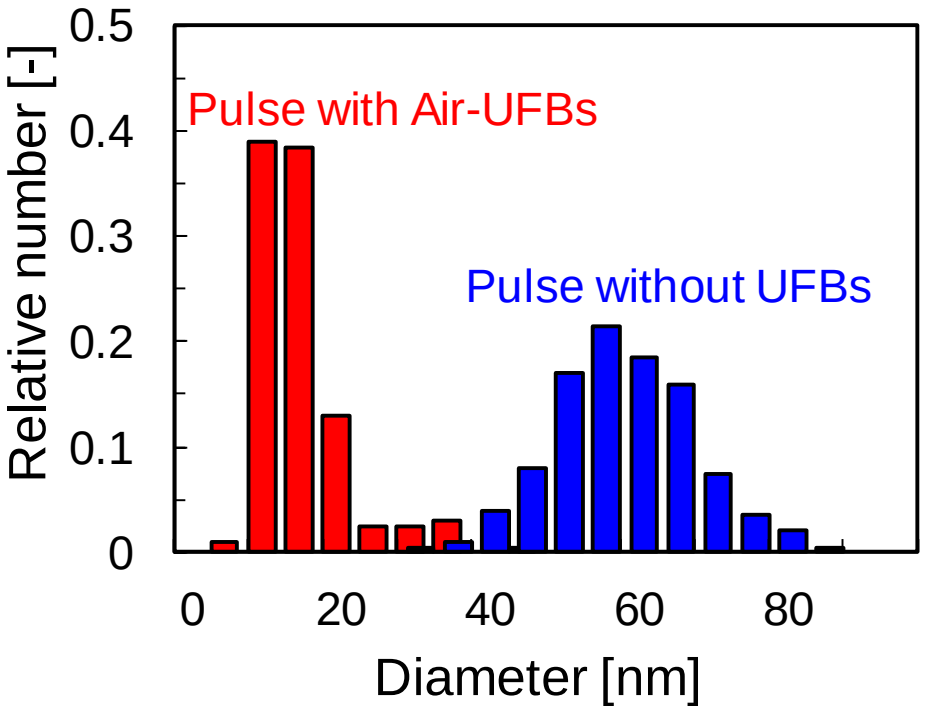

Fig. 8. (a) Electron micrographs of AuNPs and (b) diameter distribution of spherical AuNPs synthesized by pulsed ultrasound in the presence and absence of Air-UFBs.

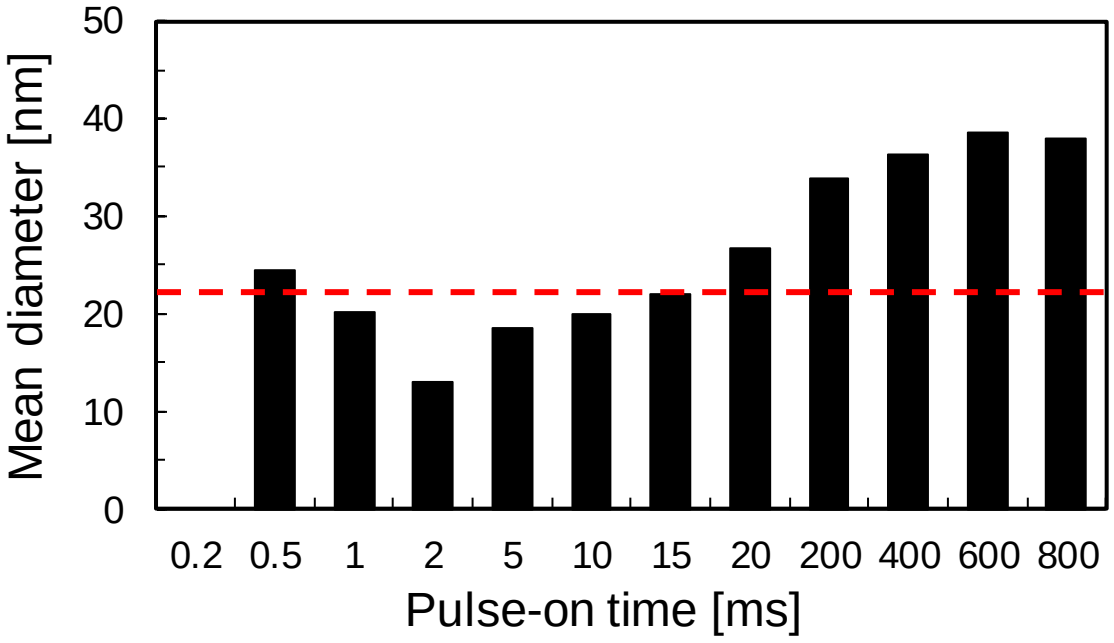

Fig. 9. Effect of pulse-on time on the mean diameter of spherical AuNPs synthesized with Air-UFBs by pulsed ultrasound. (dotted line: diameter of particles prepared under continuous-wave ultrasonication in the presence with Air-UFBs)